Preprints, Sixth Conference on Mesoscale Processes, Portland, OR, AMS, July, 18-22, 1994, pp. 335-338.

4.7 THE HEAT AND POTENTIAL VORTICITY BUDGETS OF A MIDLATITUDE SQUALL LINE

Scott A. Braun and Robert A. Houze, Jr.

Department of Atmospheric Sciences, AK-40
University of Washington
Seattle, WA 98195

1. INTRODUCTION

The effects of mesoscale convective systems on the large-scale environment are typically analyzed through budgets of heat and momentum. However, by examining these budgets separately, it can be difficult to understand fully how the convection modifies the environment. In recent years, it has become popular to examine the evolution of atmospheric flows, particularly in reference to cyclogenesis, in terms of isentropic potential vorticity (PV for short). The advantage of using PV to examine the effects of convection on the large scale is that the effects of both heating and momentum transports are "felt" by the PV. Thus, understanding how heating and momentum transports modify PV fields should lead to insights into the effects of convective processes on the larger-scale environment.

The purpose of this paper is twofold. First, we examine the heat budget for a midlatitude squall line with trailing stratiform precipitation and identify the contributions of microphysical and radiative processes to the heating within the convective and stratiform precipitation regions. Second, we examine the effects of the diabatic heating on the PV field. The effects of vertical momentum transports on the PV field will also be discussed.

2. HEAT BUDGET

In this paper, we estimate the heating rates for the 10-11 June 1985 PRE-STORM squall line (Johnson and Hamilton 1988; Rutledge et al. 1988; Biggerstaff and Houze 1991a,b, 1993; Gallus and Johnson 1991; Braun and Houze 1994a). We use a method similar to that of Houze (1982) except that observed vertical velocity data, derived from dual-Doppler radar velocity fields, are used in place of the idealized storm characteristics assumed in that study. Condensation and evaporation rates (for the sake of brevity, we include deposition and sublimation in these terms) in the convective region are estimated from

$$L\bar{c} \approx L\overline{w}_{hu}\frac{\partial \overline{q}_{hu}}{\partial z} \qquad (1a)$$

$$L\bar{e} \approx -L\overline{w}_{hd}\frac{\partial \overline{q}_{hd}}{\partial z} \qquad (1b)$$

where L is the latent heat of vaporization (sublimation) for $T>0$°C ($T<0$°C), $\overline{w}_{hu}$ and $\overline{w}_{hd}$ are the area-mean vertical motions within convective updrafts and downdrafts, respectively, $\overline{q}_{hu}$ and $\overline{q}_{hd}$ are the area-mean vapor mixing ratios in convective updrafts and downdrafts, and z is height.

In the stratiform region, we estimate the total heating from a simplified form of the thermodynamic equation

$$L\left(\bar{c}-\bar{e}\right) + L_f\left(\bar{f}-\overline{m}\right) + Q_r = \overline{w}_m\frac{\partial \overline{s}_m}{\partial z} \qquad (2)$$

where L_f is the latent heat of fusion, $\bar{f}$ and $\overline{m}$ are the mean freezing and melting rates, Q_r the mean radiative heating rate, $\overline{w}_m$ the mean vertical motion in the stratiform region, $\overline{s}_m$ the mean dry static energy, defined as $s=c_pT+gz$, c_p the specific heat at constant pressure, and g the gravitational constant. Condensation and evaporation are obtained by subtracting out the heating associated with freezing, melting, and radiative processes, which are discussed below. Equation (2) is used in the stratiform region based on heat budget estimates obtained from a numerical cloud model simulation of this squall line.

Vertical profiles of microphysical variables (cloud water/ice, rain, precipitation ice, and vapor) and melting and freezing rates are obtained by applying the one-dimensional retrieval method of Braun and Houze (1994b) to mean vertical motion profiles. [Braun and Houze (1994c) provide an in-depth examination of the melting and freezing within the 10-11 June storm.] Radiative heating rates (longwave only) are estimated by applying the two-stream plane-parallel multiband radiative transfer model of Stackhouse and Stephens (1991) to the mean vertical profiles of the microphysical variables obtained from the one-dimensional retrieval model.

Convective region vertical motion profiles are obtained from dual-Doppler velocity fields at 0131, 0139, and 0209 UTC 11 June. Stratiform region vertical motions are taken from EVAD average vertical motion profiles of Rutledge et al. (1988, see their Fig. 15). Thermodynamic conditions in the convective region are taken from the two-dimensional retrieval results of Braun and Houze (1994a), while conditions in the stratiform region are obtained by combining those retrieval results with low-level soundings (below 0°C) in the stratiform region (Braun and Houze 1994c).

Figure 1 shows vertical profiles of the heating rates, and their individual components, in the convective and stratiform regions. Figure 2 shows the total (convective+stratiform) heating by the squall line as well as comparisons of the heating profiles to the heat budget results of Gallus and Johnson (1991) for the 10-11 June storm, which were derived from composites of rawinsonde data. From these figures we can conclude the following:

- The determination of heating rates from radar data provides a better separation of the heating associated with processes in the convective and stratiform regions, compared to heating estimates

derived from composites of rawinsonde data, which lack the resolution needed to separate these components. For example, at upper levels, the total heating profiles determined from radar (BH) are in good agreement with those of Gallus and Johnson (GJ91); however, the radar-derived rates indicate that Gallus and Johnson's results attributed too much heating to the stratiform region.

- Cooling by melting in the convective (as well as the stratiform) region is an important component of the overall heat budget.

- Heating associated with radiative processes is small compared to latent heating within the convective precipitation region (Fig. 1), but is significant within a shallow layer near cloud top in the stratiform precipitation and nonprecipitating anvil regions (not shown).

3. POTENTIAL VORTICITY BUDGET

The isentropic potential vorticity (P in equations, PV in the text) equation can be written as (Holton, pg. 112, 1992)

$$\frac{\tilde{D}P}{Dt} = \frac{P}{\sigma}\frac{\partial}{\partial\theta}\left(\sigma\dot{\theta}\right) - \sigma^{-1}\mathbf{k}\cdot\nabla_\theta\times\left(\dot{\theta}\frac{\partial\mathbf{V}}{\partial\theta} - \mathbf{F}\right) \quad (3)$$

where $\tilde{D}/Dt = \partial/\partial t + \mathbf{V}\cdot\nabla_\theta$, ∇_θ is the horizontal gradient operator in isentropic coordinates, $P = \zeta_a/\sigma$, $\sigma = -g^{-1}\left(\partial\theta/\partial p\right)$, ζ_a is the absolute vertical vorticity in isentropic coordinates, θ the potential temperature, $\dot{\theta}$ is the diabatic heating rate, V the horizontal velocity in isentropic coordinates, k the vertical unit vector, and F the forcing from subgrid-scale processes. Equation (3) is similar in form to the vorticity equation in Mapes and Houze (1992), which was used to investigate the effects of diabatic heating and momentum transports on the large-scale vorticity field in the tropical Australian monsoon.

This paper provides a midlatitude counterpart for the work of Mapes and Houze (1992, 1993) by examining the effects of diabatic heating associated with the 10-11 June squall line on the large scale from a PV standpoint. In the absence of vertical wind shear and subgrid-scale forcing, changes in PV result from the "stretching" of PV and are related to the vertical gradient of diabatic heating [first term on the right side of (3)]. Such a situation was considered by Hertenstein and Schubert (1991) for simple specified distributions of diabatic heating. They did not consider the effects of vertical wind shear and subgrid-scale forcing [the second term on the right of (3)]. The part of the second term on the right involving $\dot{\theta}\partial\mathbf{V}/\partial\theta$ is the sum of the "tilting" term and vertical advection term in the isentropic coordinate system. It contains the effects of resolved momentum transports on the large-scale PV distribution. We examine this "tilting" term since the shear of V was strong in the 10-11 June storm. The effects of subgrid-scale processes (F) will be examined in future work.

To examine the effects of diabatic heating on the potential vorticity, Eq. (3) was integrated in two dimensions

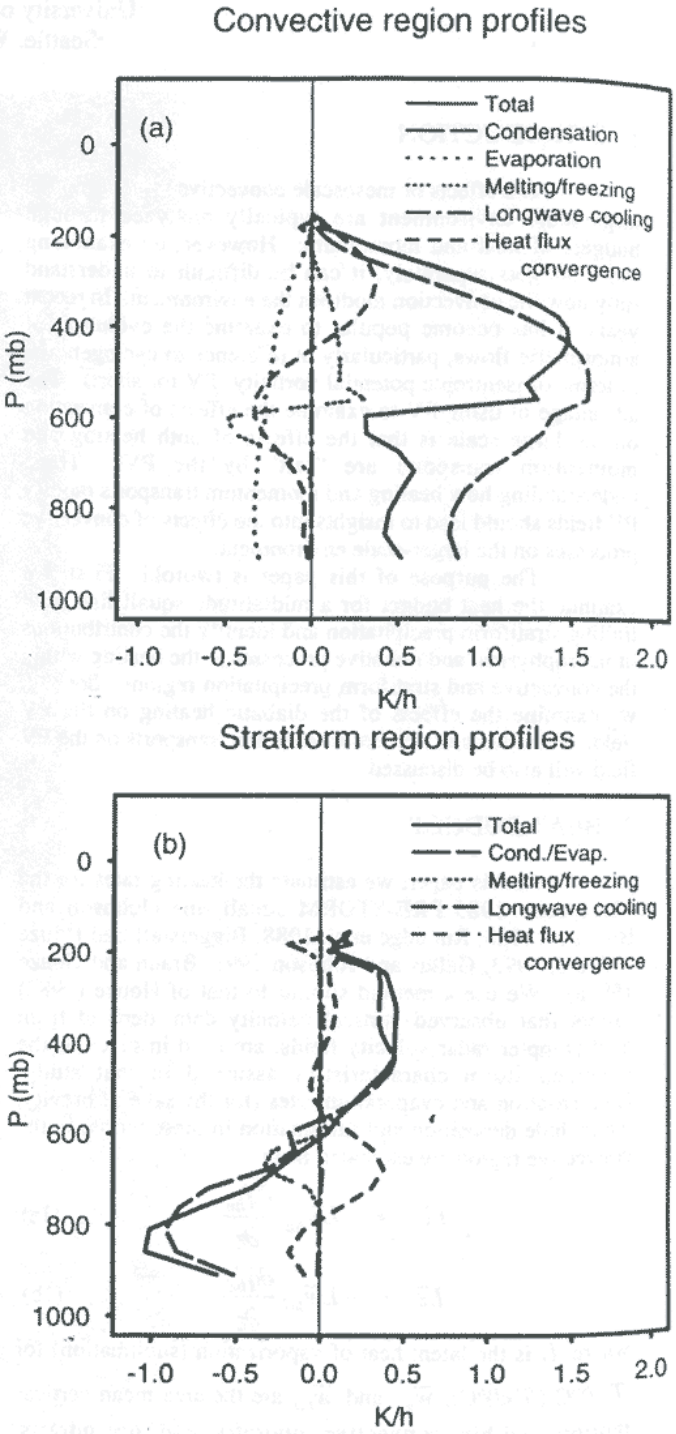

Figure 1. Vertical profiles of heating by microphysical and radiative processes, as well as eddy heat fluxes, associated with (a) the convective and (b) the stratiform precipitation regions of the 10-11 June squall line during the mature stage. The profiles represent averages over a 700 x 700 km^2 area and are normalized by the convective and stratiform fractional areas (e.g., convective area/total area), respectively.

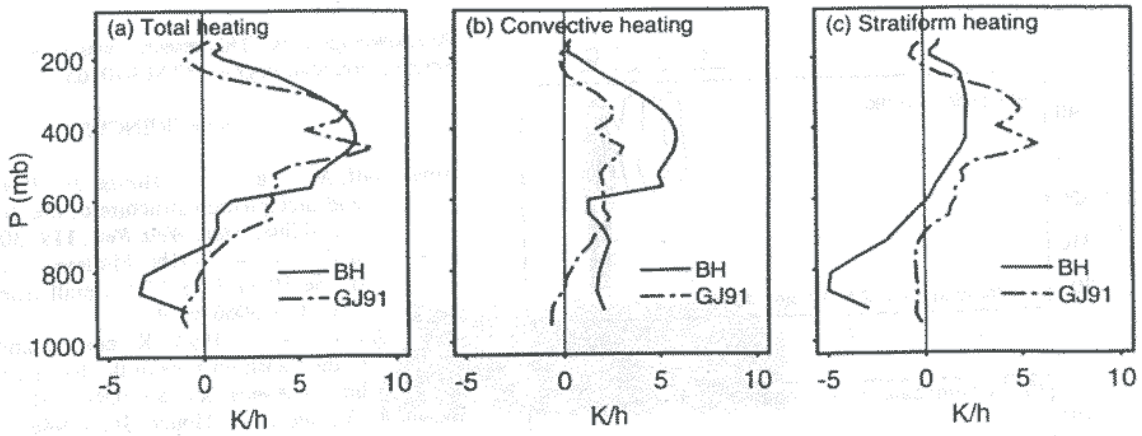

Figure 2. Comparison of the radar-derived heating rates in Fig. 1 with the rawinsonde-based profiles of Gallus and Johnson (1991). The profiles represent averages over the convective and stratiform regions only. The individual convective and stratiform components in (b) and (c) are normalized by their fractional areas [e.g., convective area/(convective + stratiform areas)].

on a grid 1600 km in length and 47 K in height, with horizontal and vertical grid spacing of 2 km and 1 K, respectively, using leap-frog time differencing, second-order centered differencing for the source terms, and fourth-order centered differencing for the horizontal advection. The heating function is specified as the sum of four components (indicated in Fig. 3a): convective, stratiform, transition (located between the convective and stratiform regions), and rear inflow (along the back edge of the stratiform region). These components are indicated by the index $i = 1, ..., 4$. The distribution of heating is then generally given by $\dot{\theta} = \sum_{i=1}^{4} G_i(x,t)F_i(\theta)$, where $G_i(x,t)$ describes the horizontal, time-dependent part of the heating and $F_i(\theta)$ specifies the vertical distribution of the heating function for component i. For this study, F_i profiles for the convective and stratiform regions are based on the diabatic heating profiles for the 10-11 June storm (Fig. 1). For the transition and rear-inflow regions, F_i is taken as a sine function. $G_i(x,t)$ is based on observations of the mesoscale circulations (Rutledge et al. 1988; Biggerstaff and Houze 1991a, 1993) and heating distribution (Gallus and Johnson 1991) associated with the 10-11 June storm. The heating function at 8 h is shown in Fig. 3a.

Two cases are examined, one without shear and a second including uniform vertical shear of the along-line wind component. P is specified initially to be uniform at 0.25 PVU (PV units, 10^{-6} m^2 s^{-1} K kg^{-1}). Figures 3b and c show cross sections of the PV perturbations (P–0.25 PVU) for the cases without and with shear after 8 h of simulation time. Only a subregion of the horizontal domain is shown. Figure 3b shows the PV perturbation field when no shear is present. Similar to Hertenstein and Schubert (1991), a midlevel PV maximum is seen near the rear of the stratiform region (x = 250 km) with a maximum value of about 3 PVU. Negative perturbations exist at lower and upper levels with values greater than –0.25 PVU. Note that the stretching term cannot produce PV perturbations less than –0.25 PVU ($P < 0$), i.e., if P is initially positive everywhere, then it will remain positive for all t if stretching is the only active process.

Figure 3c shows the PV perturbation field in the presence of shear. A midlevel PV maximum is seen near the rear of the stratiform region, as in the case without shear, but with a slightly smaller magnitude. The most significant differences between the two cases are 1) a vertical column of high PV in the convective region, 2) a region of negative PV at low levels in the stratiform region, and 3) a region of negative PV at mid-to-upper levels behind the stratiform region, which gets deformed by differential horizontal advection. A relative minimum of PV occurs within the transition region. Biggerstaff and Houze (1991) and Zhang (1992) found that the transition and stratiform regions were characterized by negative absolute vorticity (and hence, negative PV) along some portions of the squall line. While we were unable to produce negative PV values in the transition region with the simple distributions of heating and vertical shear used in our calculations, it is evident from these results that such negative values of PV can only arise in the presence of significant vertical wind shear.

Raymond (1992) suggested that the importance of shear on PV can be estimated by comparing the ratio of the vertical and horizontal scales of the heating source (h/d) to the slope of the vorticity vector, which is approximated by f/S, where f is the Coriolis parameter and S is the vertical wind shear. If $h/d >> f/S$, then the tilting dominates. For $h/d << f/S$, the stretching term dominates. For the case discussed herein, h = 47 K, d = 200 km (for the convective line and stratiform region), f = 8.6 x 10^{-5}, and S = (25 m s^{-1})/(47 K). Therefore, $h/d \approx f/S$ and both terms in (3) are important. Thus, for mesoscale convective systems in environments of moderate-to-strong shear, tilting effects will be as large as heating effects in determining the distribution of PV.

By taking the horizontal areal average of Eq. (3), one can show, however, that the tilting term vanishes in the mean when there is no heating along the domain boundaries. Thus, while tilting can significantly alter the distribution of PV, it produces no net change in the domain-averaged PV.

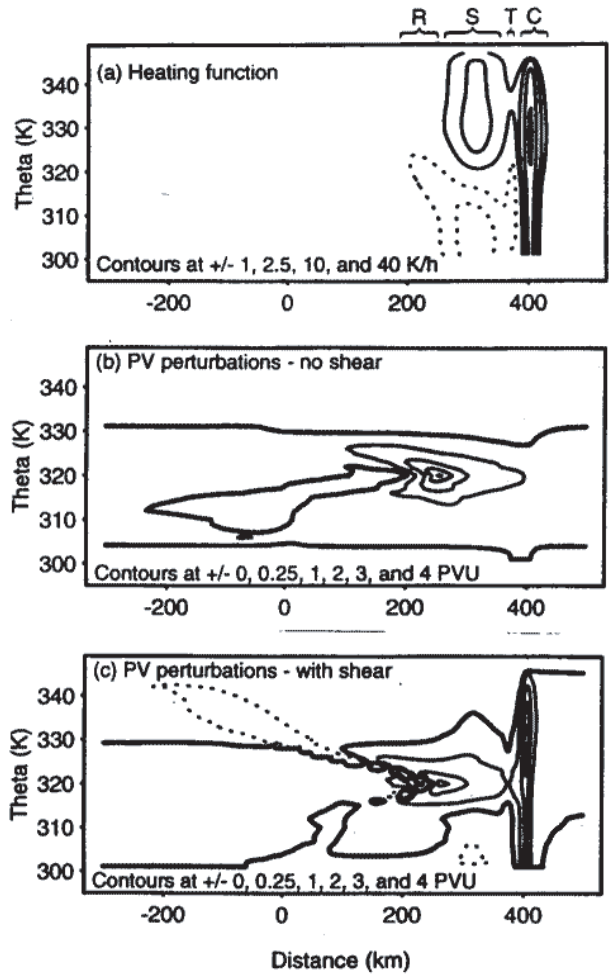

Figure 3. Diabatic heating rates (a) and PV perturbations (minus initial values) in the cases without shear (b) and including shear (c) after 8 h of simulation. Positive values are indicated by the thin solid lines and negative values by the dotted lines. Thick solid lines indicate zero values. The locations of the convective (C), transition (T), stratiform (S), and rear-inflow (R) regions are indicated at the top of the figure.

4. CONCLUSIONS

For squall lines forming in environments of moderate-to-strong vertical wind shear, changes in potential vorticity by tilting effects are as strong, or perhaps stronger, than the stretching effects associated with diabatic heating. Such tilting effects can significantly alter the horizontal distribution of PV on an isentropic surface; however, they cannot produce any net changes in the PV within regions bounding the diabatic heating. According to Eq. (3), one can directly relate the stretching and tilting effects of diabatic heating and vertical momentum transports associated with large, deep convective systems to changes in PV on an isentropic surface, which can subsequently be related to changes in the larger-scale environment.

Acknowledgments: This research was sponsored by National Science Foundation grant ATM-9101653.

REFERENCES

Biggerstaff, M. I., and R. A. Houze, Jr., 1991a: Kinematic and precipitation structure of the 10-11 June 1985 squall line. *Mon. Wea. Rev.*, **119**, 3034-3065.

———, and ———, 1991b: Midlevel vorticity structure of the 10-11 June 1985 squall line. *Mon. Wea. Rev.*, **119**, 3066-3079.

———, and ———, 1993: Kinematics and microphysics of the transition zone of the 10-11 June 1985 squall line. *J. Atmos. Sci.*, **50**, 3091-3110.

Braun, S. A., and R. A. Houze, Jr., 1994a: The transition zone and secondary maximum of radar reflectivity behind a midlatitude squall line: Results retrieved from Doppler radar data. *J. Atmos. Sci.*, (accepted).

———, and ———, 1994b: Melting and freezing in a mesoscale convective system. *Quart. J. Roy Meteor. Soc.*, (submitted).

———, and ———, 1994c: Diagnosis of hydrometeor profiles from vertical velocity data. *Quart. J. Roy. Meteor. Soc.*, (submitted).

Gallus, W. A., Jr., and R. H. Johnson, 1991: Heat and moisture budgets of an intense midlatitude squall line. *J. Atmos. Sci.*, **48**, 122-146.

Hertenstein, R. F. A., and W. H. Schubert, 1991: Potential vorticity anomalies associated with squall lines. *Mon. Wea. Rev.*, **119**, 1663-1672.

Holton, J. R., 1992: *An Introduction to Dynamic Meteorology*, Third Edition, Academic Press, 511 pp.

Houze, R. A., Jr., 1982: Cloud clusters and large-scale vertical motions in the tropics. *J. Meteor. Soc. Japan*, **60**, 396-410.

Johnson, R. H., and P. J. Hamilton, 1988: The relationship of surface pressure features to the precipitation and airflow structure of an intense midlatitude squall line. *Mon. Wea. Rev.*, **116**, 1444-1472.

Mapes, B., and R. A. Houze, Jr., 1992: An integrated view of the 1987 Australian monsoon and its mesoscale convective systems. Part I: Horizontal structure. *Quart. J. Roy. Meteorol. Soc.*, **118**, 927-963.

———, and ———, 1993: An integrated view of the 1987 Australia monsoon and its mesoscale convective systems. Part II: Vertical structure. *Quart. J. Roy. Meteorol. Soc.*, **119**, 733-754.

Raymond, D. J., 1992: Nonlinear balance and potential-vorticity thinking at large Rossby number. *Q. J. R. Meteorol. Soc.*, **118**, 987-1015.

Rutledge, S. A., R. A. Houze, Jr., M. I. Biggerstaff, and T. Matejka, 1988: The Oklahoma-Kansas mesoscale convective system of 10-11 June 1985: Precipitation structure and single-Doppler radar analysis. *Mon. Wea. Rev.*, **116**, 1409-1430.

Stackhouse, P. W., and G. L. Stephens, 1991: A theoretical and observational study of the radiative properties of cirrus: Results from FIRE 1986. *J. Atmos. Sci.*, **48**, 2044-2059.

Zhang, D.-L., 1992: Formation of a cooling-induced mesovortex in the trailing stratiform region of a midlatitude squall line. *Mon. Wea. Rev.*, **120**, 2763-2785.